Supporting Information

Coupling confinement activating cobalt oxide for high-turnover electrocatalytic overall water splitting

Linlin Cao[‡a], Yuanjie Cao[‡a], Xiaokang Liu[a], Qiquan Luo[b], Wei Liu[a], Wei Zhang[a], Xiaoli Mou[a], Jinlong Yang[b], Tao Yao*[a], Shiqiang Wei[a]

[a] National Synchrotron Radiation Laboratory, University of Science and Technology of China. Hefei 230029, P. R. China.

[b] Hefei National Laboratory for Physical Sciences at the Microscale.

Contents

EXPERIMENTAL METHODS

XAFS measurements and data analysis

The acquired EXAFS data were processed according to the standard procedures using the ATHENA module implemented in the IFEFFIT software packages[1]. The k^3-weighted $\chi(k)$ data in the k-space ranging from 2.5–10.5 Å^{-1} were Fourier transformed to real (R) space using a hanning windows ($dk = 1.0$ Å^{-1}) to separate the EXAFS contributions from different coordination shells. To obtain the detailed structural parameters around Co atom in the as-prepared samples, quantitative curve-fittings were carried out for the Fourier transformed $k^3\chi(k)$ in the R-space using the ARTEMIS module of IFEFFIT[2]. Effective backscattering amplitudes $F(k)$ and phase shifts $\Phi(k)$ of all fitting paths were calculated by the ab initio code FEFF8.0[3]. The Co_3O_4 bulk comprises two types of geometrical cobalt sites with different oxidation states: one Co(II) in the tetrahedral site and two Co(III) in the octahedral site, according to the standard crystal structure. Considering the coordination bond length of Co(II)-O (1.928 Å) is similar to that of Co(III)-O (1.917 Å), therefore, a three-shell structure model including a single Co-O and two separate Co-Co shells was used to fit the EXAFS data. The coordination numbers (CN) were fixed accordingly, while other structural parameters, such as interatomic distance (R), and the Debye-Waller factor (σ^2) were allowed to vary. As for the CoOx/PCN sample, the FT curves showed comparable coordination peak positions with that of Co_3O_4, except for significantly damped peak intensity. Therefore, the same three-shell structure

model was used in the fitting analysis. Of note, the Debye–Waller factor (σ^2) of two Co-Co shells were set equal in order to reduce the number of adjustable fitting parameters. The other structural parameters, such as interatomic distance (R), and the Debye–Waller factor (σ^2) were allowed to vary.

Turnover frequency (TOF) calculation.

The OER-TOF per Co site of the CoO_X/PCN electrocatalyst was calculated according to the following equation:

$$TOF(O_2) = \frac{\#\,Total\,oxygen\,turnovers\,per\,geometric\,area}{\#\,active\,sites\,per\,geometric\,area} \qquad S(1)$$

The number of total oxygen turnovers per geometric area was calculated from the current density for the OER-LSV polarization:

Total oxygen turnovers per geometric area

$$= (|J|\frac{mA}{cm^2})(\frac{1C/s}{1000mA})(\frac{1\,mol\,e^-}{96453.8C})(\frac{1\,mol}{4e^-})(\frac{6.023\times10^{23}}{1\,mol\,O_2})$$

$$= 1.56\times10^{15}\,\frac{O_2/s}{cm^2}\,per\,\frac{mA}{cm^2} \qquad S(2)$$

The number of Co atoms number in CoO_x/PCN catalyst were calculated from the Co molar mass and the mass loading ($m_{Loading}$) on the GC electrode, which derived from the ICP. Assuming each cobalt atoms in the catalyst formed one active center. The Co content of catalyst revealed by ICP-AES measurement was 1%, thus, the mass loading is 0.283 mg/cm^2.

The upper limit of active site density is:

$$\text{Co atoms number} = (\frac{m_{\text{Loading}}(\text{x g/cm}^2) \times \text{Co wt\%}}{\text{Co M}_w \text{ (g/mol)}}) \times (\frac{6.022 \times 10^{-3} \text{Co atoms}}{1 \text{mol Co}})$$

$$= (\frac{0.283 \times 10^{-3} \text{ g/cm}^2 \times 1 \text{wt\%}}{58.93 \text{ g/mol}}) \times (\frac{6.022 \times 10^{-3} \text{Co atoms}}{1 \text{mol Co}})$$

$$= 2.89 \times 10^{16} \text{ Co site per cm}^2 \qquad\qquad \text{S(3)}$$

Finally, the current density from the OER-LSV polarization curve can be converted into values according to:

$$\text{TOF}_{\text{OER}} = (\frac{1.56 \times 10^{15}}{2.89 \times 10^{16}} \times |J|) = 0.05|J| \qquad\qquad \text{S(4)}$$

Particularly, at the overpotential of 300 mV, the current density of OER is 33.8. Therefore, the TOF values of CoO_x/PCN electrocatalyst were calculated to be:

$$\text{TOF}_{\text{OER}} = 0.05|J| = 1.69 \text{ O}_2 \text{ s}^{-1} \qquad\qquad \text{S(5)}$$

Mass activity calculation.

Mass activity (A g^{-1}) was derived from the current density (mA cm^{-2}) that normalized by the mass loading (mg cm^{-2}) at a special overpotential. As the following equation exhibited:

$$\text{Mass activity} = (|J| / \text{Mass loading}) = 3.58 |J| \qquad\qquad \text{S(6)}$$

When OER were tested at the overpotential of 350 mV, the current density is 74.05 mA cm^{-2}, therefore, the mass activity were calculated to be:

$$\text{Mass activity }_{\text{OER}} = 3.58 |J| = 3.58 \times 74.05 = 265.10 \text{ A/g.} \qquad \text{S(7)}$$

COMPUTATIONAL METHODS and MODELS

All calculations were performed using the plane-wave periodic density functional method (DFT)in the Vienna *ab initio* simulation package (VASP).[4,5] The electron ion

interaction was described with the projector augmented wave (PAW) method.[6,7] The electron exchange and correlation energy was treated within the generalized gradient approximation (GGA) in the form of the Perdew-Burke-Ernzerh of (PBE) functional.[8] The van der Waals interactions were described by the empirical correction in Grimme scheme (vdW-D3).[9] The cut-off energy was set up to 500 eV. The force convergence was set to be lower than 0.02 eV/Å, and the total energy convergence was set to be smaller than 10^{-5} eV. Electron smearing of $\sigma = 0.1$ eV was used following the the Gaussian scheme. Brillouin zone sampling was employed using a Monkhorst-Pack grid.[10]

The adsorption energy of an intermediate A adsorption on the model is defined as $E_{ads} = E_{(model+A)} - (E_A + E_{model})$, where $E_{(model+A)}$ is the total energy of the model with adsorbate A, E_{model} is the total energy of the bare model and, E_A is the total energy of isolated adsorbate A. Therefore, the more negative the adsorption energy, the stronger the adsorption. For modelling the experimental catalyst CoO_x/PCN *i.e.*, CoO_x nanoclusters confined on (PCN) support, a ball-like $Co_{28}O_{26}$ cluster with size of greater than 10 Å in diameter was chosen to mimic the CoO_x nanocluster; and a single layerperiodic slab with (4×4) supercell g-C_3N_4 with a P atom substituting ternary C atoms was utilized to model the PCN. To anchor the $Co_{28}O_{26}$ cluster on the PCN strongly, two neighboring O atom between the cluster and PCN interface were removed, and the optimized model was shown in Fig. S17c, all the atoms in the model were fully released and the vacuum slab was set up to 15 Å. The model has more coordination-unsaturated surface Co atoms compared with Co_3O_4 bulk material. In

addition, the A termination of the Co_3O_4 (110) surface [Co_3O_4 (110)-A], which expose

both types of Co^{2+} (tetrahedral, three-fold Co_{3f}) and Co^{3+} (octahedral, four-fold Co_{4f})

ions at the surface, was built to model the Co_3O_4 bulk material (d). Co_3O_4 (110)-A has

periodic slab with (1×1) supercell, and atoms at top three layers were relaxed and

bottom three layers were fixed at their bulk positions, and the vacuum slab was also

set up to 15 Å.
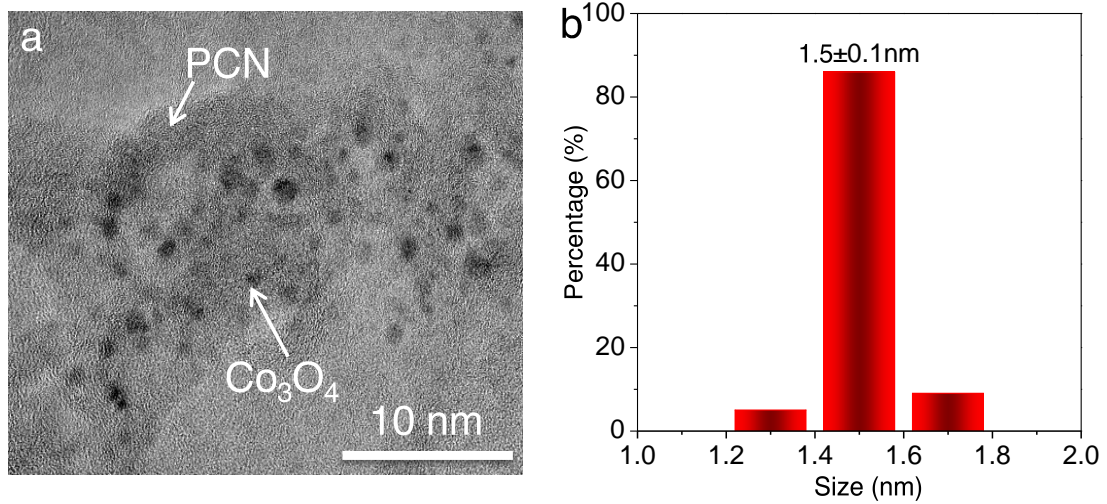
Fig. S1. (a) TEM image and corresponding (b) size distribution of as-obtained CoO_x/PCN electrocatalyst.
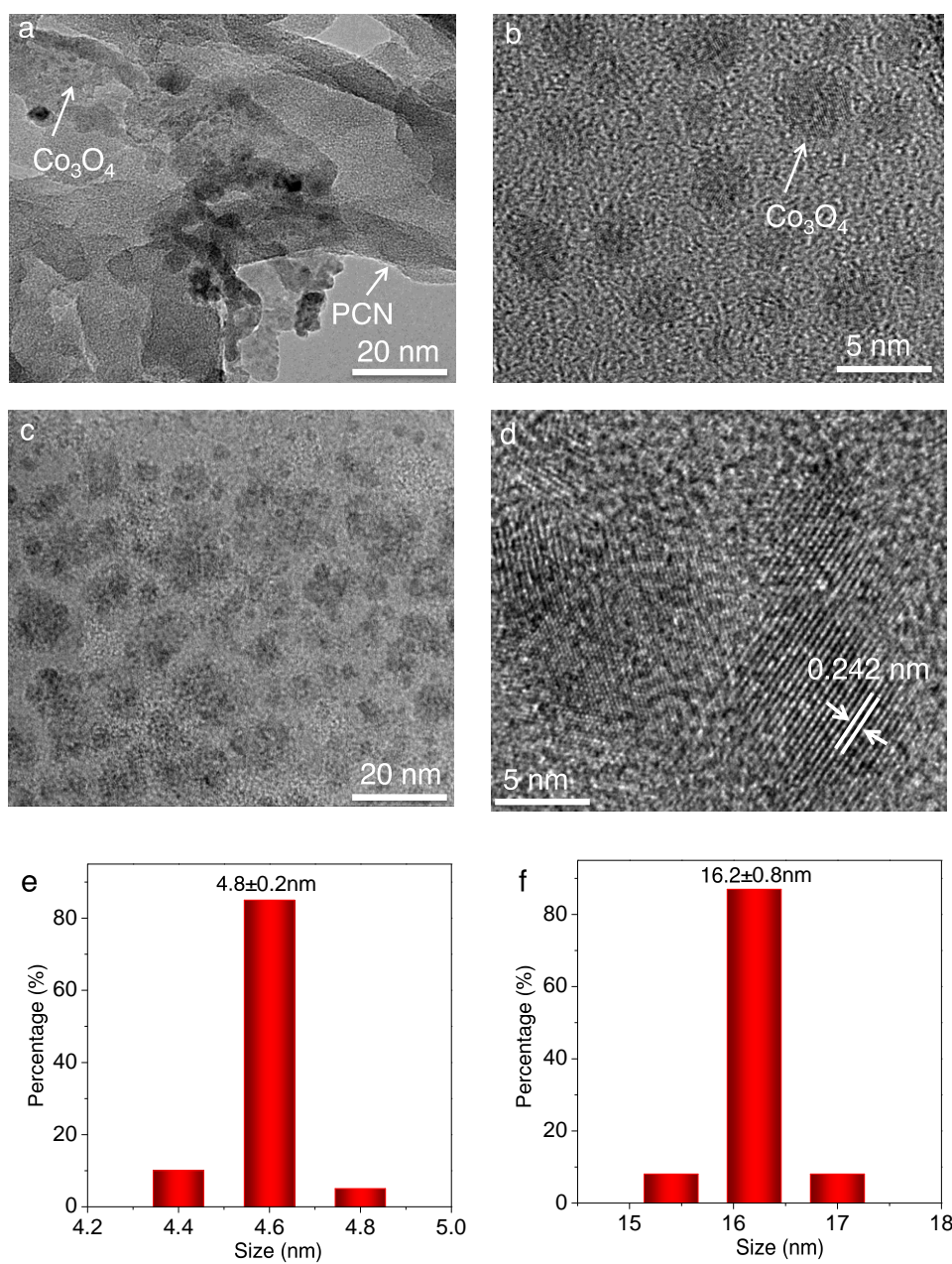
Fig. S2. (a), (c) Low magnification, (b), (d) high magnification TEM images and corresponding size distribution of as-obtained Co_3O_4 NP/PCN and Co_3O_4 +PCN, respectively.
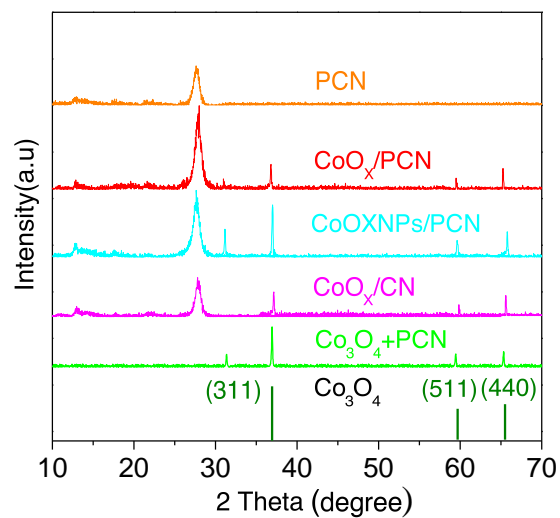
Fig. S3. Experimental XRD pattern of the as-synthetized PCN, CoO$_x$/PCN, CoO$_x$ NP/PCN, CoO$_X$/C$_3$N$_4$, Co$_3$O$_4$+PCN and the standard pattern of Co$_3$O$_4$. The sharp peaks at 36.9, 59.4 °, and 68.6 ° corresponds to the (311), (511) and (400) lattice planes of cubic Co$_3$O$_4$, indicating the formation of Co$_3$O$_4$ clusters.
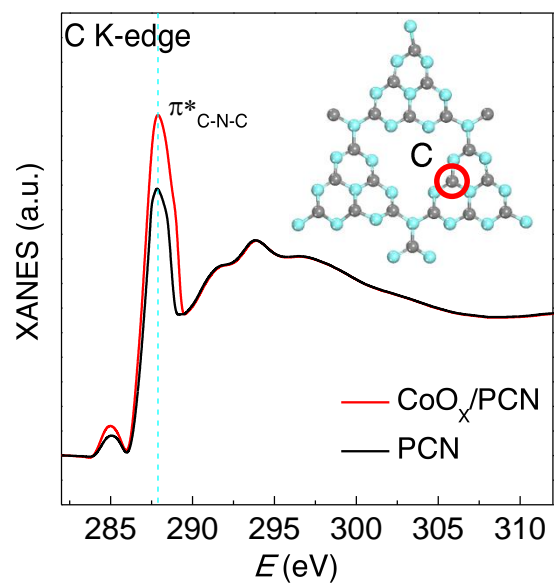
Fig. S4. C K-edge XANES spectra of CoO$_x$/PCN and PCN.
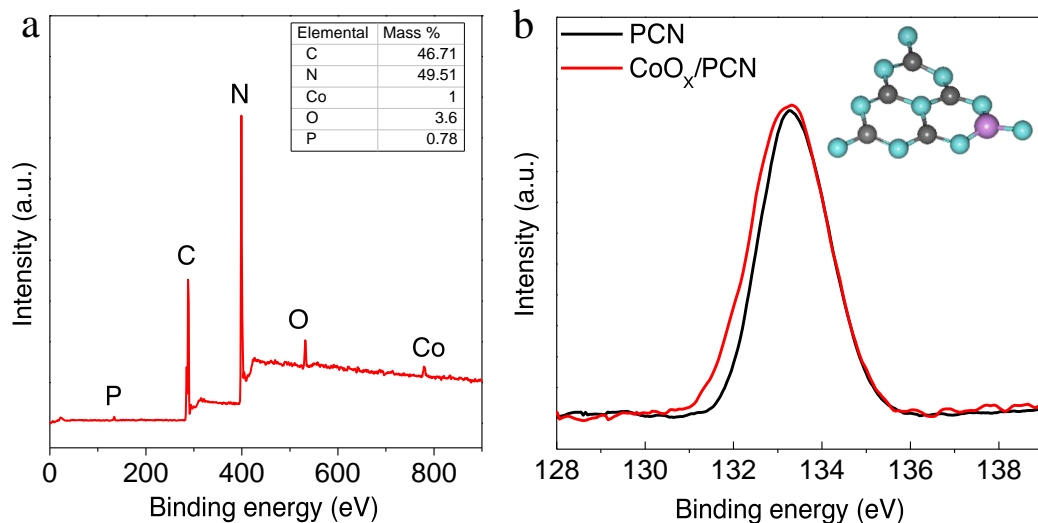
Fig. S5. (a) XPS survey spectrum of CoO$_x$/PCN sample. The XPS survey spectrum indicates that the sample only contains C, N, O, Co and P without anything else impurities. (b) The P $2p$ XPS spectra of the CoO$_x$/PCN sample displayed one peak at 133.1 eV peak that is characteristic of P-N coordination (P-O bonding would be approximately 1 eV higher and P-C be around 1–2 eV lower), indicating the substitution of P for C atoms in triazine rings of g-C$_3$N$_4$[1].
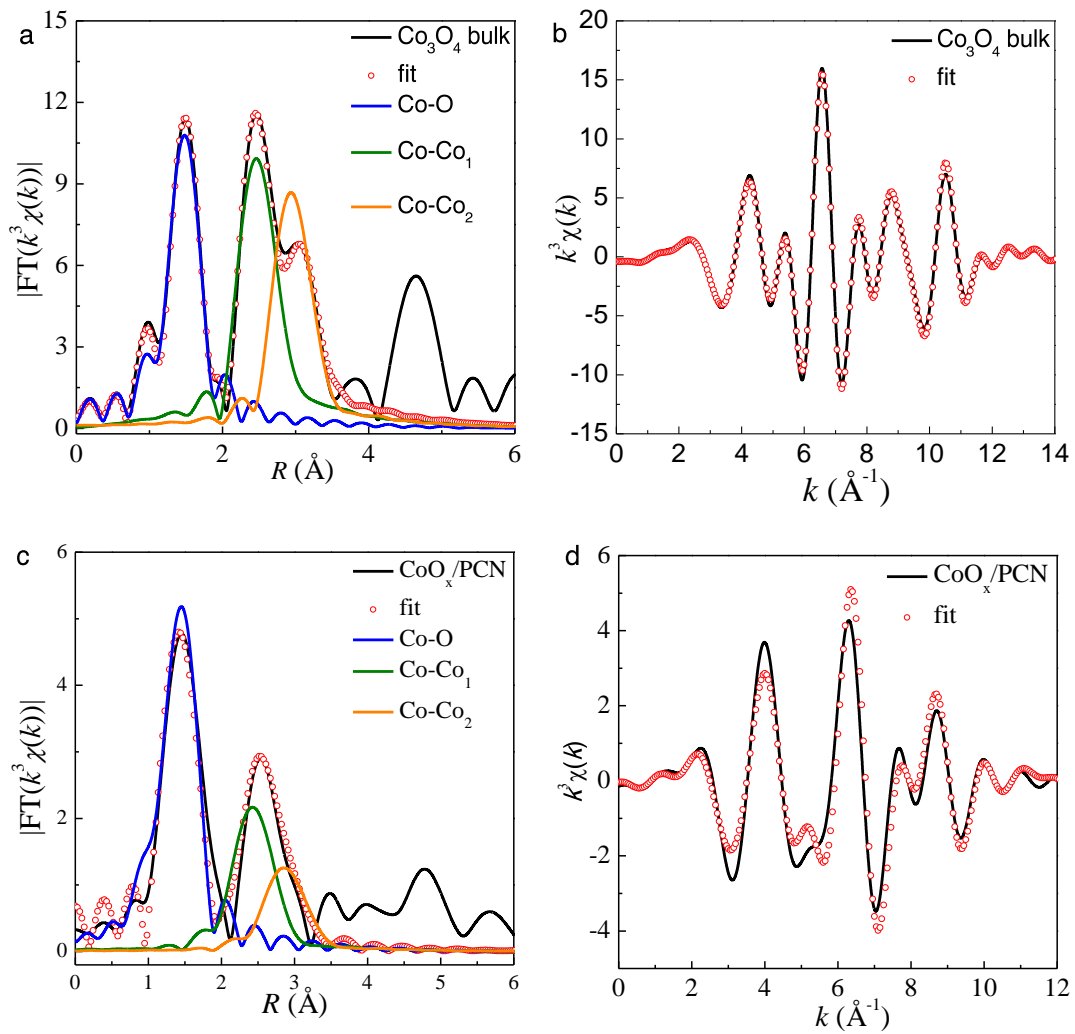
Fig. S6. The fitting curve of k^3-weighted EXAFS spectra and $k^3\chi(k)$ oscillations of Co_3O_4 (a-b) CoO_x/PCN (c-d) sample.
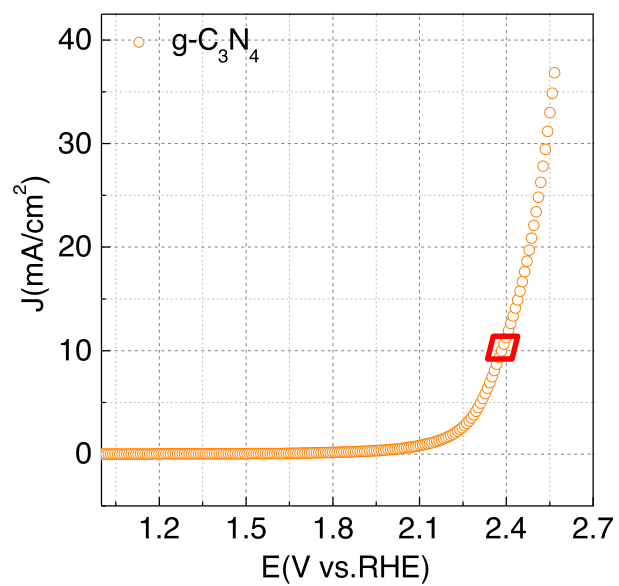
Fig. S7. LSV of OER of the C_3N_4 in 1.0 M KOH, this result indicates that g-C_3N_4 is inactive for OER.
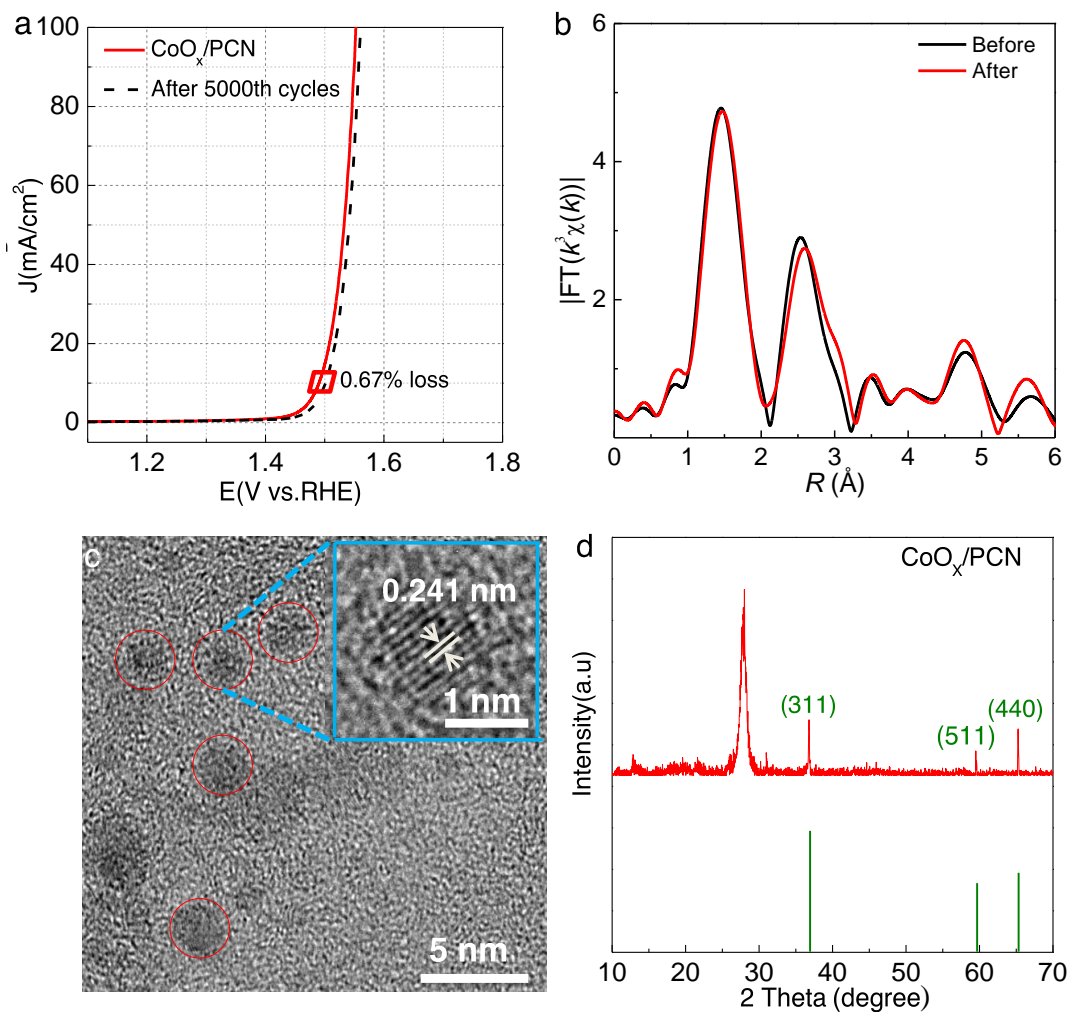
Fig. S8. (a) Initial and after 5000th CV cycles OER-LSV of the CoOx/PCN sample in 1.0 M KOH, There is unconspicuous positive (0.67% loss) for OER LSV curves after 5000th CV cycles test. (b) The corresponding k^3-weighted Fourier transform spectra from extended X-ray absorption fine structure before and after electrochemical test. (c)TEM and HRTEM (insert) images and (d) XRD pattern of CoOx/PCN after 5000th CV cycles. The size and structure of the CoOx/PCN nearly unchanged after electrochemical test. The typical lattice fringe of 2.41 Å that is belong to (311) lattice plane of Co_3O_4, moreover, the diffraction peaks of (311), (511), and (440) of cubic Co_3O_4 also detected.
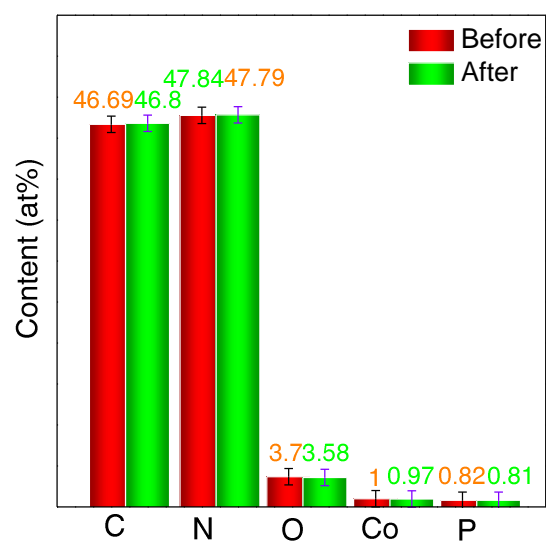
Fig. S9. Inductively coupled plasma atomic emission spectrometry (ICP-AES) of the CoO$_x$/PCN electrocatalyst before and after electrochemical test. (Red represents before test and green represents the catalyst after test). The results pointed out the mass loading of Co on PCN is about 1%, with consistent to the amount of the precursor, moreover, a unmarked mass content of Co change has taken place after electrochemical test, meaning outstanding stability.
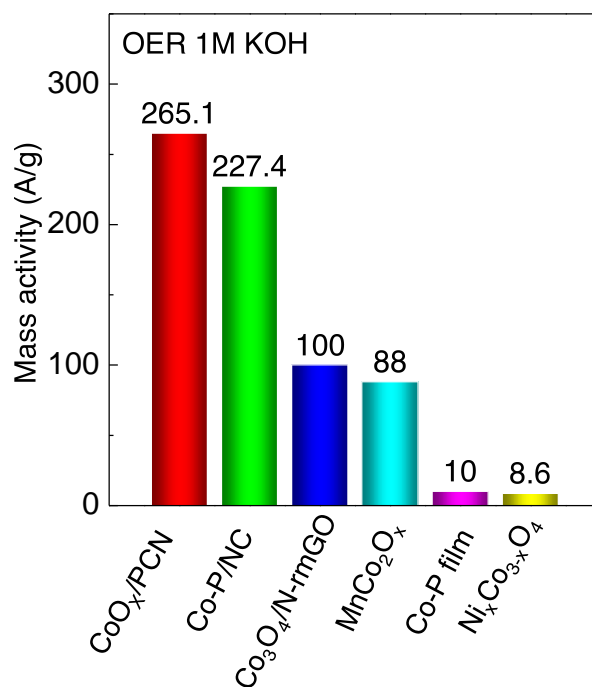
Fig. S10. Mass activity of the CoO$_x$/PCN electrocatalyst for OER at overpotential of 350 mV. To the best of our knowledge, the mass activity of the CoO$_x$/PCN electrocatalyst compares to most of recently reported catalysts. (Co-P/NC[2], Co$_3$O$_4$/N-rmGO[3], MnCo$_2$O$_x$[4], Co-P film[5], Ni$_x$Co$_{3-x}$O$_4$[6], CoP/CC[7], Co-S/FTO[8], Ni$_2$P[19], MoB[20], FeP NAs/CC[9]).

a CoOx/PCN

b Cdl=45.6 mF/cm²

c CoOxNP/PCN

d Cdl=25.7 mF/cm²

e CoOx/C3N4

f Cdl=10.1 mF/cm²
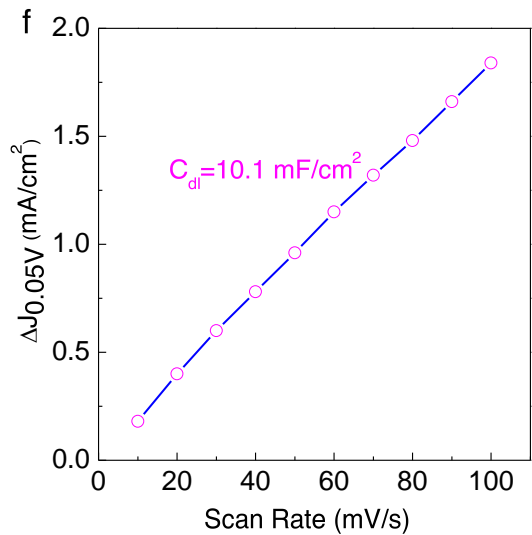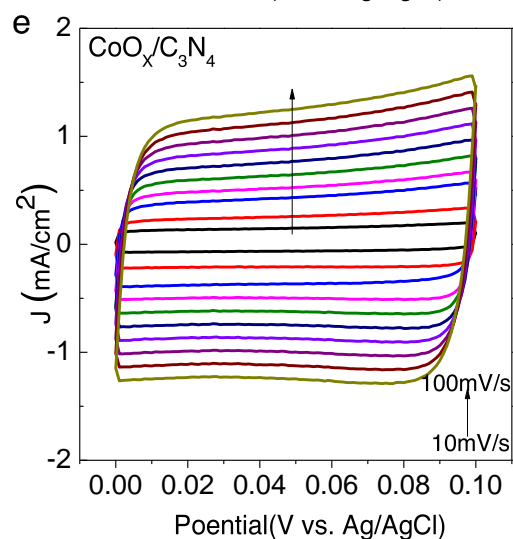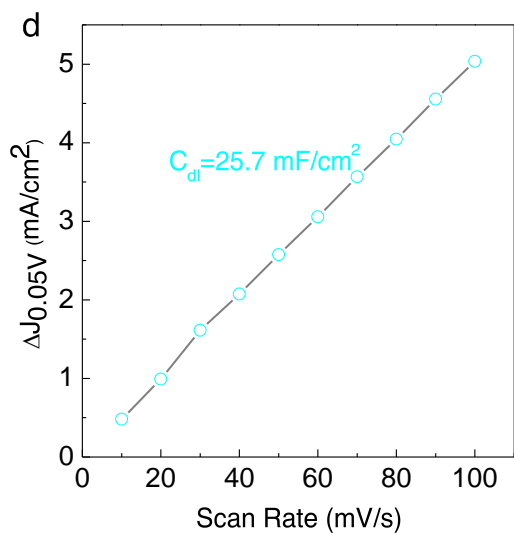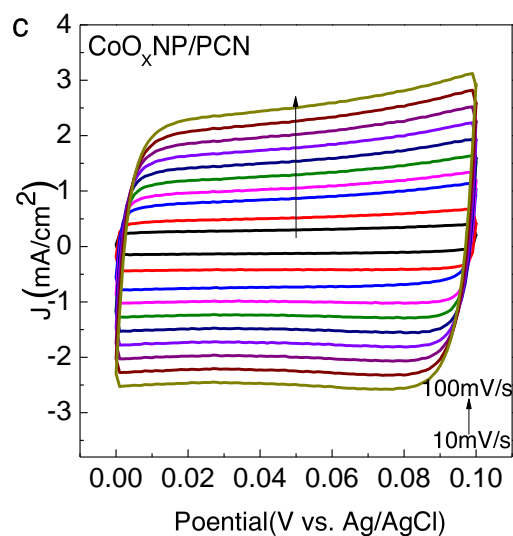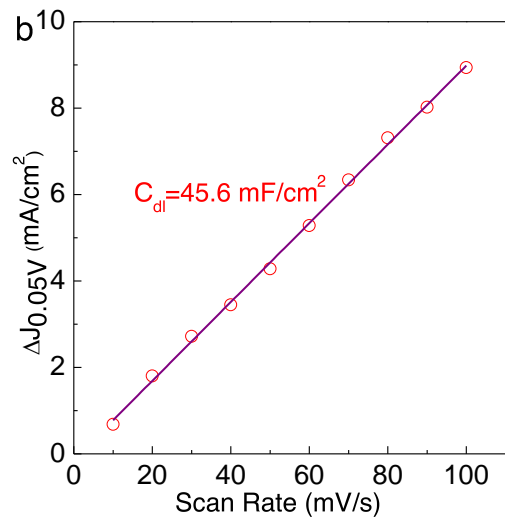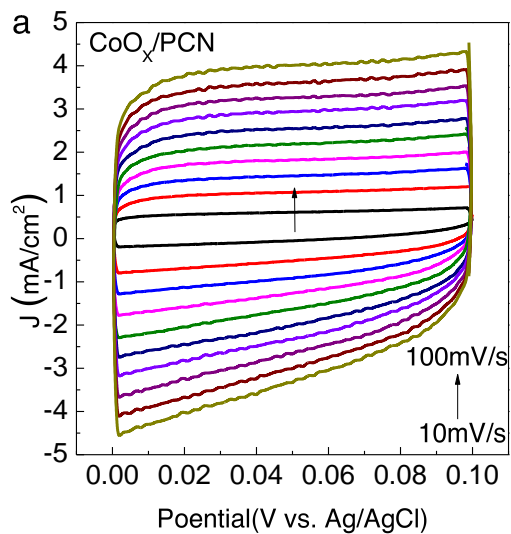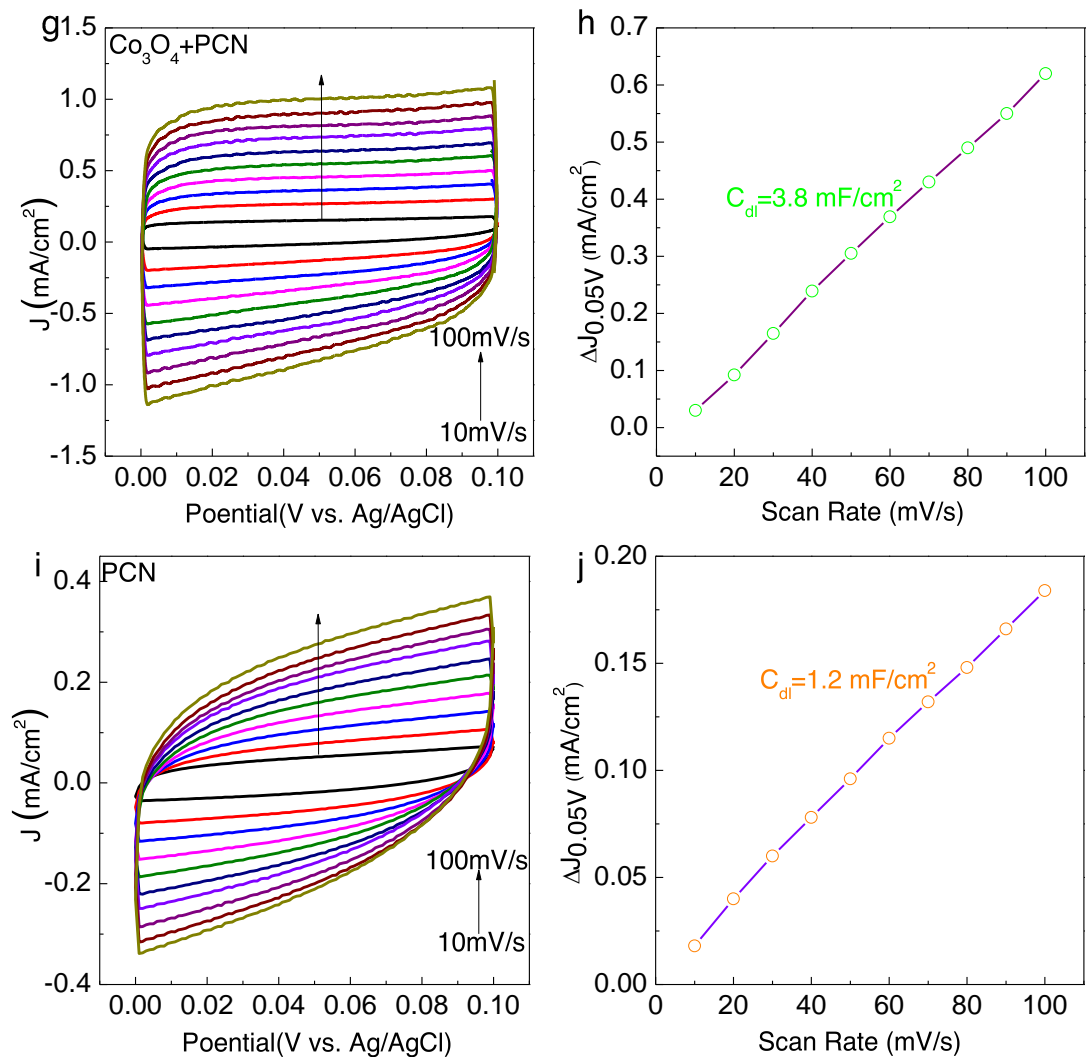
Fig. S11. (a), (c), (e), (g), (i) Cyclic voltammetry curves of CoO$_X$/PCN, CoO$_X$ NP/PCN, CoO$_X$/C$_3$N$_4$, Co$_3$O$_4$+PCN and PCN in the voltage range of 0-0.1V vs. Ag/AgCl at various scan rates (10, 20, 30 mV s^{-1}, ect); (b), (d), (f), (h), (j) estimate the electrochemical double layer capacitance (C$_{dl}$) and relative electrochemically active surface area; The C$_{dl}$, which is expected to be linearly proportional to the effective electrochemical active area, was also carried out using a simple cyclic voltammetry (CV) method to estimate the effective surface areas of the solid-liquid interface of the different kinds of catalysts. Current response was taking in the potential window for the CV (0–0.1 V vs.RHE) with different scan rates (0–100 mV s^{-1}) should only be due to the charging of the double-layer without any Faradaic current.
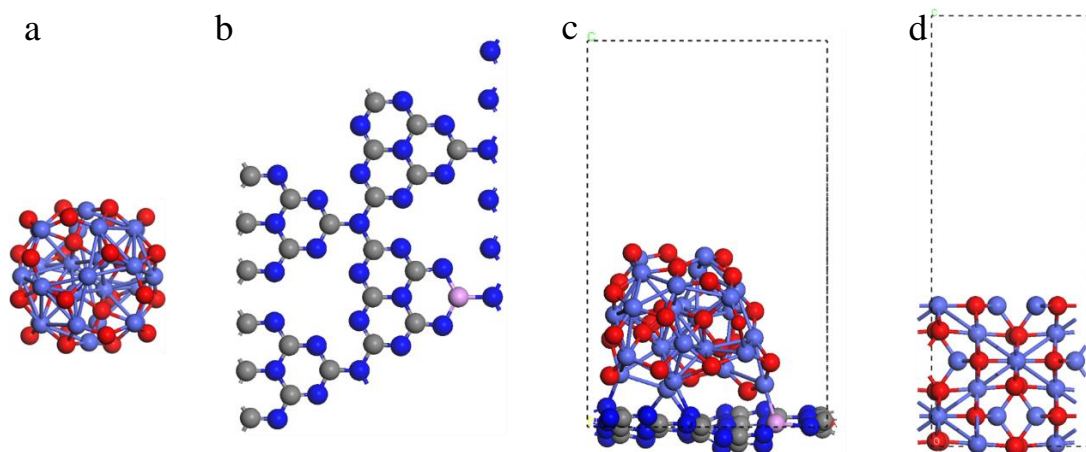
Fig. S12. The configurations of $Co_{28}O_{26}$ cluster (a) PCN (b) and CoO_x/PCN (c), and Co_3O_4 (110)-A (d). O atom in red, Co atom in light blue, N atom in dark blue, C atom in gray and P atom in pink. H_2O and OH adsorption on Co_3O_4 (110)-A and CoO_x/PCN were calculated and the optimized configurations were shown in Fig. 4e and 4f. H_2O favors to bond to the Co_3O_4 (110)-A surface atop, with O atom coordinating a surface Co_{3f} atom and O-Co_{3f} titled the surface. The computed O-Co_{3f} bond distance is 2.05 Å and the adsorption energy is of -1.22 eV. The values are agreement with those of computed at GGA+U lever (2.07 Å vs.-1.02 eV) by Selloni group.[10] OH has a bidentate adsorbed configuration on the Co_3O_4 (110)-A surface. O atom of OH group bonds to two surface neighboring Co_{4f} atoms, and the formed O-Co_{4f} bond distances are of 1.93 and 1.94 Å, respectively. The adsorption energy is of -4.20 eV. H_2O prefer to bond to a less coordinated (four-fold) Co atom atop, and the former Co-O bond is 2.26 Å in length, which is around 0.20 Å longer than that of H_2O adsorption on Co_3O_4 (110)-A. The calculated adsorption energy is of -2.70 eV, indicating a much stronger adsorption on the CoO_x/PCN than on Co_3O_4 (110)-A. OH favors atop adsorption on a five-fold Co atom. The O-Co bond distance is of 1.78Å, and the adsorption energy is -5.42 eV, which is around 1.20 eV lower than that of on Co_3O_4 (110)-A. The computed results reveal that both H_2O and OH have much stronger adsorption on CoO_x/PCN than on Co_3O_4 (110)-A.

Table S1. Structural parameters extracted from quantitative EXAFS curve-fitting using the ARTEMIS module of IFEFFIT.

Sample	Path	N	R (Å)	σ^2 (10^{-3}Å^2)	ΔE_0 (eV)	R-factor
Co_3O_4	Co-O	5.3	1.92±0.01	2.8±0.3	-0.1±0.6	0.0001
	Co-Co$_1$	4.0	2.85±0.01	3.0±0.4	-1.4±1.0	
	Co-Co$_2$	9.3	3.36±0.02	6.9±0.5	-1.4±1.0	
	Co-O	4.6±0.4	1.94±0.02	7.0±0.6	-7.0±1.0	0.0102
CoO_x/PCN	Co-Co$_1$	2.9±0.4	2.90±0.03	11.0±1.2	-7.5±1.5	
	Co-Co$_2$	2.5±0.4	3.35±0.04	11.0±1.2	-7.5±1.5	

N, coordination number; R, bonding distance; σ^2 Debye-Waller factor; ΔE_0 inner potential shift;

Table S2. OER activities of the CoO_x/PCN and the reported catalysts in alkaline solution at 10 mA cm^{-2}.

Ctalysts	Mass loading (mg/cm^2)	Overpotential (mV)	Tafel slope (mV dec^{-1})	References
CoO_x/PCN	0.28	269	60	Our work
γ-CoOOH nanosheets	0.28	300	38	*Angew. Chem. Int. Ed.* 2015, *127*, 8846-8851
IrO_2/C	0.2	370	/	*Nat. Commun.*, 2013, *4*, 2390.
$Co-C_3N_4/CNT$	0.22	380	68.4	*J. Am. Chem. Soc.* 2017, *139*, 3336-3339.
Co/CoP	0.22	340	79.5	*Adv. Energy. Mater.* 2017, *7*, 1602355
CoO-CNF	0.6	340	73.6	*Nat. Commun.*, 2015, *6*, 7261.
Co phosphade (PCPTF)	0.1	330 (J=30mA cm^{-2})	65	*Adv. Mater.*, 2015, *27*, 3175-3180.
Co-P film	2.52	345	47	*Angew. Chem. Int. Ed.*, 2015, *127*, 6349-6352.
NiFe-LDH	0.07	302	40	*Nat. Commun.*, 2014, 5, 4477.
Co_3O_4/N-rmGO	1.0	310	67	*Nature Mater.*, 2011, *1108*, 2331.
CoMn LDH	0.142	340 mV (J=25mA cm^{-2})	43	*J. Am. Chem. Soc.*, 2014, *136*, 16481-16484.
NiFe-LDH/CNT	0.25	308	31	*J. Am. Chem. Soc*, 2013, *135*, 8452-8455.
$Au@Co_3O_4$	0.2	500 (J=25mA cm^{-2})	60	*Adv. Mater.*, 2014, 26, 3950-3955.
$Ni_x Co_{3-x}O_4$	2.3	430 (J=30mA cm^{-2})	64	*Adv. Mater.*, 2010, *22*, 1926-1929.
VOOH	0.8	270	68	*Angew. Chem. Int. Ed.*, 2017, *129*, 588-592.
MoS_2/Ni_3S_2	9.7	218	88	*Angew. Chem. Int. Ed.*, 2016, 128, 6814-6819.
Co_3O_4/C	0.2	290	70	*J. Am. Chem. Soc.*, 2014, *136*, 13925-13931.
$Mn_3O_4/CeSe_2$	0.2	450	49	*J. Am. Chem. Soc.*, 2012, *134*, 2930-2933.
$g-C_3N_4-CNT$	0.2	370	83	*Angew. Chem. Int. Ed.*, 2014, *53*, 2930-2933.

Table S3. Fitted values of the EIS data of OER process at the overpotential of 300 mV.

Catalysts	R_{ct} (Ω)	R_s (Ω)
CoO_x/PCN	79.28	9.62
CoO_x NP/PCN	314.40	9.45
CoO_x/C_3N_4	358.57	10.58
CoO_x +PCN	483.27	10.79
PCN	2028.46	10.26

Supplementary references

1 Y. Zhang, M. Antonietti, *J. Am. Chem. Soc.* 2010, **5**, 1307.

2 B. You, N. Jiang, M. Sheng, S. Gul, J. Yano, Y. Sun, *Chem. Mater.* 2015, **27**, 7636.

3 Y. Liang, Y. Li, H. Wang, J. Zhou, J. Wang, T. Regier, H. Dai, *Nat. Mater.* 2011.

4 F. Song, X. Hu, *J. Am. Chem. Soc.* 2014, **136**, 16481.

5 L. Trotochaud, J. K. Ranney, K. N. Williams, S. W. Boettcher, *J. Am. Chem. Soc.* 2012, **134**, 17253.

6 Y. Li, P. Hasin, Y. Wu, *Adv. Mater.* 2010, **22**, 1926.

7 J. Tian, Q. Liu, A. M. Asiri, X. Sun, *J. Am. Chem. Soc.* 2014, **136**, 7587.

8 Y. Sun, C. Liu, D. C. Grauer, J. Yano, J. R. Long, P. Yang, C. J. Chang, *J. Am. Chem. Soc.* 2013, **135**, 17699.

9 Y. Liang, Q. Liu, A. M. Asiri, X. Sun, Y. Luo, *ACS Catal.* 2014, **4**, 4065.

10 J. Chen, A. Selloni, *J. Phys. Chem. Lett.* 2012, **3**, 2808.